Research Article Vol. 2, No. 6 / June 2015 / Optica 547

Orbital angular momentum vertical-cavity surface-emitting lasers

Huanlu Li,[1,2] David B. Phillips,[3,4,6] Xuyang Wang,[1] Ying-Lung Daniel Ho,[1] Lifeng Chen,[1] Xiaoqi Zhou,[3] Jiangbo Zhu,[5] Siyuan Yu,[1,5] and Xinlun Cai[5,7]

[1]Department of Electrical and Electronic Engineering, University of Bristol, University Walk, Bristol BS8 1TR, UK
[2]School of Engineering, Rankine Building, Oakfield Avenue, University of Glasgow, Glasgow G12 8LP, UK
[3]H.H. Wills Physics Laboratory, University of Bristol, Tyndall Avenue, Bristol BS8 1TL, UK
[4]Department of Physics and Astronomy, University of Glasgow, Glasgow G12 8QQ, UK
[5]State Key Laboratory of Optoelectronic Materials and Technologies and School of Physics and Engineering, Sun Yat-sen University, Guangzhou 510275, China
[6]e-mail: david.phillips@glasgow.ac.uk
[7]e-mail: caixlun5@mail.sysu.edu.cn

Received 2 March 2015; revised 19 May 2015; accepted 22 May 2015 (Doc. ID 235395); published 4 June 2015

Harnessing the orbital angular momentum (OAM) of light is an appealing approach to developing photonic technologies for future applications in optical communications and high-dimensional quantum key distribution (QKD) systems. An outstanding challenge to the widespread uptake of the OAM resource is its efficient generation. In this work we design a new device that can directly emit an OAM-carrying light beam from a low-cost semiconductor laser. By fabricating micro-scale spiral phase plates within the aperture of a vertical-cavity surface-emitting laser (VCSEL), the linearly polarized Gaussian beam emitted by the VCSEL is converted into a beam carrying specific OAM modes and their superposition states, with high efficiency and high beam quality. This new approach to OAM generation may be particularly useful in the field of OAM-based optical and quantum communications, especially for short-reach data interconnects and QKD.

OCIS codes: (050.4865) Optical vortices; (140.7260) Vertical cavity surface emitting lasers; (130.3120) Integrated optics devices; (140.3300) Laser beam shaping.

http://dx.doi.org/10.1364/OPTICA.2.000547

1. INTRODUCTION

Optical beams with phase singularities, also known as optical vortices, were first discussed by Nye and Berry in 1974 [1], who identified singularities within randomly scattered fields. In 1992, Allen *et al.* recognized that orbital angular momentum (OAM) is a natural characteristic of all helically phased light beams, and could be readily generated in a standard optics lab [2]. Beams carrying OAM are attractive as they offer a theoretically unbounded number of possible states, and have therefore been a subject of great interest for a variety of fundamental and applied research activities at both the classical and the single-photon level. Applications include communication [3], optical manipulation [4], optical microscopy [5], remote sensing [6], and quantum information [7]. Beams with a well-defined state of OAM have a complex field characterized by $\exp(il\varphi)$, where φ is the azimuthal around the optical axis, and l is the topological charge, an integer describing the number of 2π phase changes around the beam axis. Such beams can be created by imposing an azimuthally dependent phase structure onto the beam. This is routinely achieved by using bulk optical components such as spatial light modulators (SLMs). Despite offering great flexibility, SLMs suffer a slow response time limited to milliseconds, and have no clear route to miniaturization. In emerging OAM-based classical or quantum information systems utilizing optical fibers [8] or free-space [9] transmission, a key requirement is integrated components that generate OAM-carrying beams in a compact and cost-effective way.

Recently, several silicon photonics integrated OAM emitters, which convert planar waveguide modes into free-space OAM modes [10–12], have been reported as potential candidates for future communication systems. These are significantly more compact and robust than their bulk optics counterparts. However, as passive devices, they require external lasers sources, which not only increases the cost and the complexity but also reduces the power efficiency, which can be critical for many applications [3,8,9]. Therefore, power-efficient active OAM-emitting devices that can be fabricated in large quantities at low cost, and can form integrated emitter arrays, are highly desirable.

Here, we report a novel approach to generating specific OAM-carrying beams by integrating micro-sized spiral phase plates (SPPs) in the aperture of vertical-cavity surface-emitting lasers (VCSELs). The VCSEL device represents an attractive light source in many industrial applications due to its low fabrication cost, high energy efficiency, circularly symmetric beam profile,

and high intrinsic modulation bandwidths [13,14]. There has also been intense research into the use of VCSEL-like devices as single-photon sources [15] and as low-cost sources in quantum key distribution (QKD) systems [16]. By integrating VCSELs with our additional phase structures, high-purity OAM modes and their superposition states can be generated while maintaining advantages in cost and power efficiency. Photonic components can be produced, which are highly suitable not only for OAM-based optical communications systems, but also for quantum systems [17,18].

2. VCSEL DEVICES AND FABRICATION OF SPPS

Figure 1(a) illustrates the structure of a commercially available single-mode and linearly polarized VCSEL that has been integrated with an SPP. The laser consists of an active lasing region sandwiched between two distributed Bragg reflector (DBR) mirrors. The devices include a nano-grating in their aperture surface for polarization control so that linearly polarized beams are emitted. In the unmodified device, when electric current is injected through the top P-contact and the bottom N-contact, a Gaussian beam is emitted from the aperture at a wavelength of 860 nm with a typical threshold current of 1 mA. A maximum output power of 4 mW can be achieved with an injected current of 6 mA. Figure 1(b) shows an SEM image of the aperture of an unmodified VCSEL with a diameter of 8.5 μm.

An l-fold helical phase front can be imprinted on the emitted beam by fabricating a SPP in the aperture of the VCSEL. Figure 1(c) shows a sketch of a SPP, which imparts the desired helical phase term, $\exp(il\varphi)$, by possessing a dielectric layer of graduated thickness that varies with the azimuthal angle around the center of the plate. Spiral phase shift sectors with a 0–2π phase variation can be achieved, and are repeated l times (where $l = +3$ in the case of Fig. 1(c)). In our stepped SPP design, the total phase

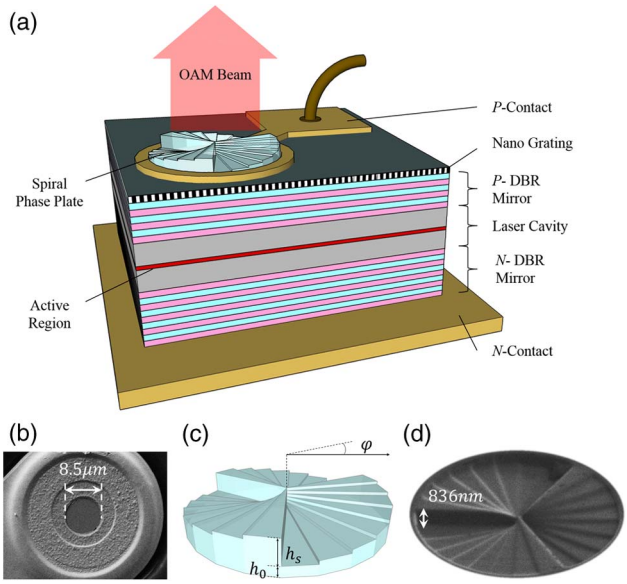

Fig. 1. Structure of the VCSEL device with integrated SPP. (a) schematic of the VCSEL device with an integrated SPP; (b) SEM image of the aperture of the VCSEL device before SPP fabrication; (c) sketch of a stepped SPP with topological charge of $+3$. h_s is the total step height, and h_0 is the base height of the plate. (d) SEM image of the fabricated stepped SPP.

shift of 2π is divided into eight equally spaced discrete levels within each phase shift sector. To achieve a full 2π phase shift, the height required is $\lambda/(n_r - n_0)$, where n_r is the refractive index of the SPP material and n_0 is the refractive index of the surrounding medium. Therefore the total step height of the SPP, h_s, is given by $(N-1)\lambda/N(n_r - n_0)$, where N is the number of levels (eight in this case). From Fig. 3(c) it can be seen that $h_s = 836$ nm (using $n_r = 1.9$ for silicon nitride, $n_0 = 1$, $\lambda = 860$ nm, and $N = 8$). Figure 1(d) shows an SEM image of an etched SPP ($l = +3$), where the multisector, multistep SPP structures are displayed. The SPPs were fabricated in a 1000 nm thick silicon nitride film deposited on the top of the VCSEL and patterned using a focused ion beam (FIB) etching technique (see Supplement 1).

3. STRUCTURES AND TOPOLOGICAL CHARGE MEASUREMENT RESULTS

The fabricated SPPs in the aperture of the VCSEL with various OAM mode orders are pictured in Figs. 2(a1), 2(b1), 2(c1), and 2(d1). The light–current (L-I) curves and spectral characteristics of the VCSEL devices remain unchanged after the SPP fabrication process. We image the farfield intensity distribution of the generated OAM beams. For $l = 0$, as shown in Fig. 2, row a, the emitting area is only covered by the silicon nitride film, so the farfield of the generated beam remains Gaussian. We included this modification to demonstrate that the addition of a dielectric layer on top of the VCSEL had no adverse effect on its operation. For devices with a SPP of nonzero topological charge, annular intensity distributions are observed, as displayed in Figs. 2(b2), 2(c2), and 2(d2). These intensity distributions are in good agreement with those expected of optical vortex modes as given by semianalytical simulations of light emitted from VCSELs integrated with eight stepped SPPs [Figs. 2(b3), 2(c3), and 2(d3)] (see Supplement 1). As expected, higher values of the topological charge, l, yield larger diameter annular farfield intensity distributions, and exhibit a dark spot on the optical axis due to the phase singularity at the vortex core. The simulated spiral phase patterns of the farfield are illustrated in Figs. 2(b4), 2(c4), and 2(d4). It can be observed that the number of the helical arms is equal to the number l of the helical phase front of the OAM beam.

The emitted beams are further characterized using computed holograms displayed on a SLM to confirm their topological charge. The liquid-crystal-based SLM has dimensions of 7.68 mm × 7.68 mm, 512 × 512 pixels, and a working wavelength range of 760–865 nm. The optical setup to perform the beam OAM analysis is shown in Fig. 2(e) [19]. The VCSEL emitter is placed at the front focal plane of the objective lens, which produces the Fourier transform of the emitted beam in its back focal plane. This plane is then reimaged to the plane of the SLM using a 4f imaging system (lenses 1 and 2). The half-wave plate is used to rotate the polarization of the linearly polarized transmitted light to the correct orientation for the polarization-dependent SLM. After diffraction by the SLM, there is another 4f system (lenses 3 and 4) to magnify the beam before it is imaged onto the CCD camera using lens 5.

In order to measure the OAM spectrum (which represents the relative mode content) of the generated beams, we sequentially display a series of forked phase holograms on the SLM. Each possesses a topological charge of l', which imparts an additional phase term of $\exp(il'\varphi)$ to light diffracted from the SLM into the first order of the diffraction pattern. Figures 2(f)–2(i) show the intensity distributions of the beams diffracted from the SLM, emitted

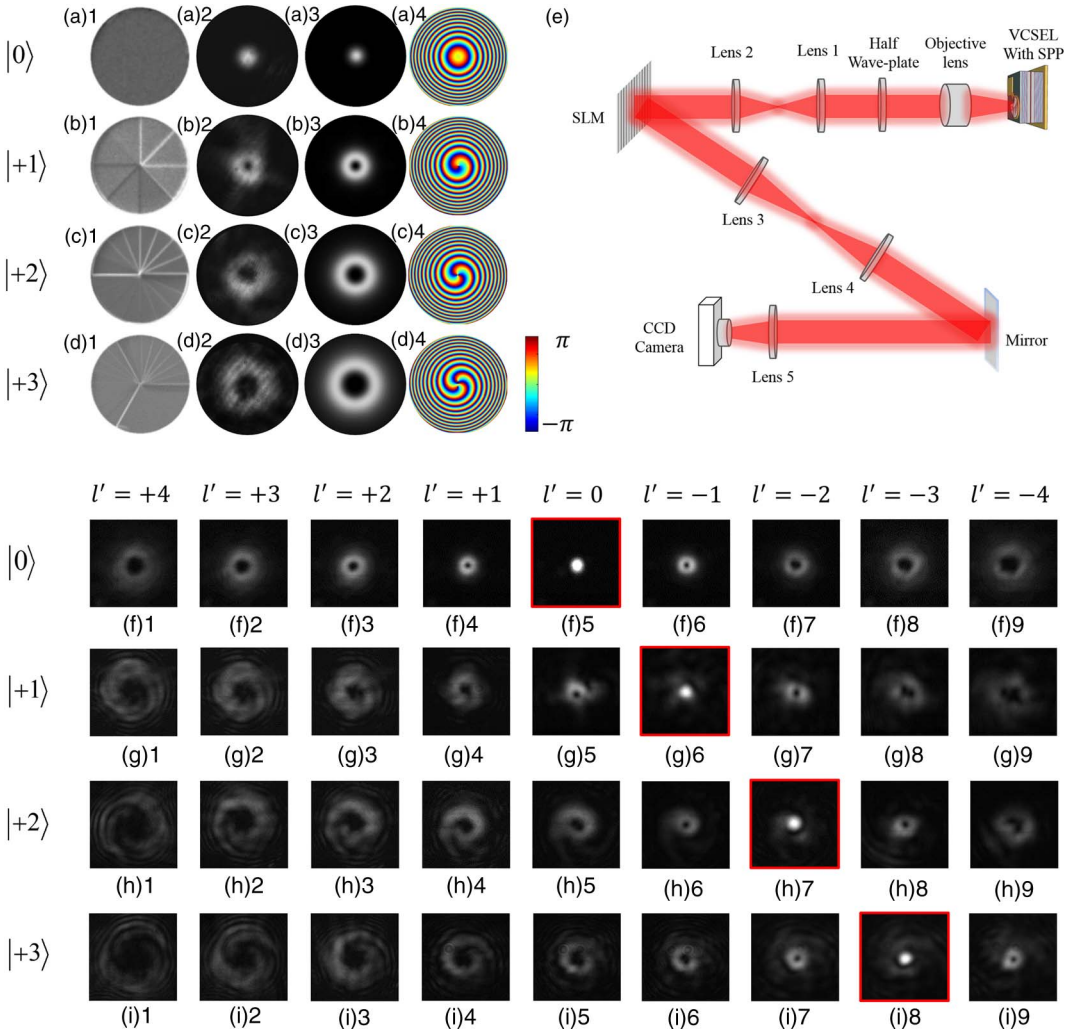

Fig. 2. Experimental and simulation results of the OAM beams. (a1, b1, c1, d1) top view SEM images of the fabricated SPP; (a2, b2, c2, d2) experimentally observed intensity profiles of the generated OAM beams from the SPP; (a3, b3, c3, d3) simulated intensity profiles of the OAM beams; (a4, b4, c4, d4) simulated phase patterns of the OAM beams; (e) experimental setup for characterization of OAM modes; (f)–(i) intensity profiles of the OAM beam diffracted by the SLM.

by VCSELs integrated with SPPs of $l = 0, +1, +2$, and $+3$. The obtained images represent OAM beams with a topological charge of $l' + l$. When an optical vortex beam of topological charge l is incident upon the SLM with a forked phase mask of topological charge $l' = -l$, a Gaussian beam is transmitted into the first-order diffraction pattern, and the annular intensity distribution is replaced with that of a Gaussian beam with a peak intensity on axis (and therefore a bright spot at the center). In the cases of $l' \neq -l$, the annular farfield intensity distribution is due to an OAM beam of order $l' + l$. As an example, Fig. 2, row g, shows the transmitted beam from a VCSEL integrated with a SPP of topological charge $l = +1$, and Figs. 2(g1)–2(g9) show the measured intensity distributions after the beam has diffracted from the SLM displaying holograms of $l' = -4$ to $l' = +4$. In Fig. 2(g6), where $l' = -1$, the transmitted beam contains a bright spot (indicating a major Gaussian component of the beam) on axis at the center of the image.

In addition to the generation of individual OAM states, a key strength of our approach is that we can further design composite SPPs that can generate beams carrying a superposition of multiple well-defined OAM states. For example, a concentric SPP consisting of an inner region with a SPP of topological charge $l = +1$ surrounded by an outer region with a SPP of topological charge $l = -2$, can be used to convert the Gaussian beam of the VCSEL into superposition states of $|+1\rangle$ and $|-2\rangle$, as shown in Figs. 3(a1) and 3(b1). By setting the diameter of the inner region of the SPP to 3.8 μm (to be compared with the VSCEL total aperture diameter of 8.5 μm) as shown in Fig. 3(d), an equal weighting of the $|+1\rangle$ and $|-2\rangle$ components can be achieved as they each intercept an equal amount of light energy flux (this diameter is indicated by the dashed black line). Furthermore, by changing the relative orientation of the inner and outer regions of the SPP, the relative phase of $|+1\rangle$ and $|-2\rangle$ components can be tuned from 0 to 2π.

The interference patterns of two OAM modes generated by conventional approaches have been demonstrated before [20–23], and produce "petal" patterns with a number of lobes equal to the modulus of the difference in topological charge between the two interfering beams. In our case this is equal to l_{inner}-l_{outer}. To demonstrate this we constructed two composite SPPs that can generate superpositions of $(|+1\rangle + |-2\rangle)$ and $(|+1\rangle - |-2\rangle)$, respectively, as shown in Figs. 3(a) and 3(b). In Figs. 3(a2) and

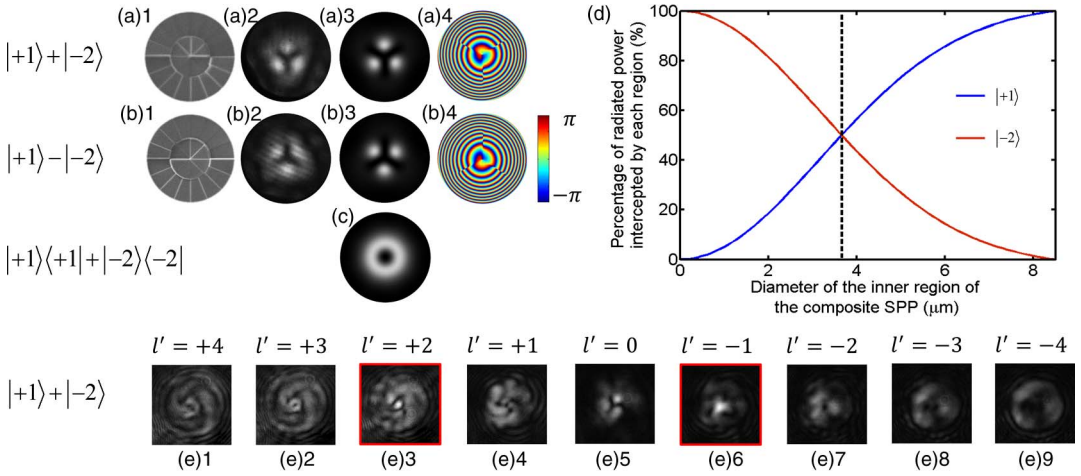

Fig. 3. Experimental and simulated results of OAM beams with superposition states. (a1, b1) top view SEM images of the fabricated SPP; (a2, b2) observed intensity distributions of the generated OAM beams from the SPPs; (a3, b3) simulated intensity distributions of the OAM beams; (a4, b4) simulated phase patterns of the OAM beams; (c) simulated intensity distribution of a mixed OAM state; (d) OAM mode purities with the ratio of diameter of the inner SPP; (e) beam patterns of the OAM beam diffracted from the SLM.

3(b2), petal-like intensity patterns are observed, which agree very well with the numerical simulations presented in Figs. 3(a3) and 3(b3). The presence of the petalled intensity distributions is a signature of the interference of the beams and the presence of a superposition state of coherent modes. This can be contrasted with Fig. 3(c), which shows a simulation of the intensity distribution formed by an incoherent mixture of states, which is a sum of the individual intensities (hence no interference) rather than a sum of their complex fields.

We again used the setup shown in Fig. 2(e) to characterize the OAM spectra of the beams generated from VCSELs integrated with the composite SPPs shown in Figs. 3(a1) and 3(b1). The resulting intensity distribution for a VCSEL with a composite SPP of a superposition state ($|+1\rangle + |-2\rangle$) is shown in Fig. 3, row e. As expected, now on-axis central bright spots can be observed for two values of l' displayed on the measurement SLM [Figs. 3(e3) and 3(e6)], corresponding to SLM topological charge of $l' = -1$ and $l' = +2$. This indicates the simultaneous presence of the two OAM states.

The generation of OAM superposition states demonstrates our integrated OAM VCSEL device as a promising candidate for OAM-based quantum communication systems. For example, there are three mutually unbiased bases for a two-dimensional system, which in our case can be defined by the normalized bases [24]: basis $1 = [|+1\rangle, |-2\rangle]$; basis $2 = [(1/\sqrt{2})(|+1\rangle + |-2\rangle), (1/\sqrt{2})(|+1\rangle - |-2\rangle)]$; and basis $3 = [(1/\sqrt{2})(|+1\rangle + i|-2\rangle), (1/\sqrt{2})(|+1\rangle - i|-2\rangle)]$. For clarity, these are analogous to the three mutually unbiased polarization state bases (also a two-dimensional system) defined by left circular and right circular polarization, horizontal and vertical polarization, and diagonal and antidiagonal polarization. However, as our system is composed of spatial modes, the unlimited value that can be taken by the topological charge l, means that it is readily extended beyond two-dimensional QKD protocols to higher-dimensional quantum systems [25,26].

By measuring the on-axis intensity in the farfield intensity distributions as the SLM hologram is sequentially varied through a range of values of l' [27], the relative power in each of the conjugate modes $l' = -l$ can be inferred, yielding the OAM spectrum of the generated beams (see methods in Refs. [3,28] for more detail). As can be seen in Figs. 2(g)–2(i) and 3(e), some degradation of beam quality can be observed. The measured spectra display a small amount of power in OAM modes adjacent to the desired mode. This can also be seen from the presence of low-intensity rings surrounding the on-axis light in images in Fig. 3. In theory, the SPP is not a pure OAM mode converter [29], and the discrete nature of the stepped SPP results in a small degradation in beam purity, depending on the number of the steps in one phase sector [30]. However, this is a small effect, and Fig. 4 presents the simulated and measured mode purities for OAM beams generated by the VCSELs with different topological charges. The simulated OAM mode purity and weight values are calculated by the overlap-integral method [31,32] (see Supplement 1). In the case of $l = 0$, the measured purity of the OAM mode is approximately 95%, which can be attributed to factors such as limited flatness of the silicon nitride film, in addition to any aberrations within the optical system [3]. The measured mode purity values for $l = +1$, $l = +2$, and $l = +3$ are 89%, 84%, and 78% compared with the simulation results of 98%, 99%, and 99%, respectively. In terms of the superposition OAM state, as shown in Fig. 4(e), the mode energy is nearly equally distributed into $|+1\rangle$ and $|-2\rangle$ with the values of 34% and 38%, respectively, while the corresponding simulated values are both 49%. The two experimental values sum to 82%, which is similar to that of 84% obtained with the single $l = +2$ mode.

In the measured results, mode purity degradation could arise from rotational symmetry-breaking factors, such as the nonideal intensity distribution of the emitted beam from the VCSEL (i.e., deviation from Gaussian distribution), any small misalignments between the optical axis of the VCSEL and SPP's centers [3], and imperfections in the SPP fabrication. Also any small misalignments in the optical system will cause spreading of power into nearby modes [33]. Therefore, the measured purity of OAM modes is limited as a result of the generation of unwanted modes due to these nonideal factors [34]. The mode impurity resulting from the VCSEL and SPP itself could be further improved by more accurate control over the height of each step in the SPP

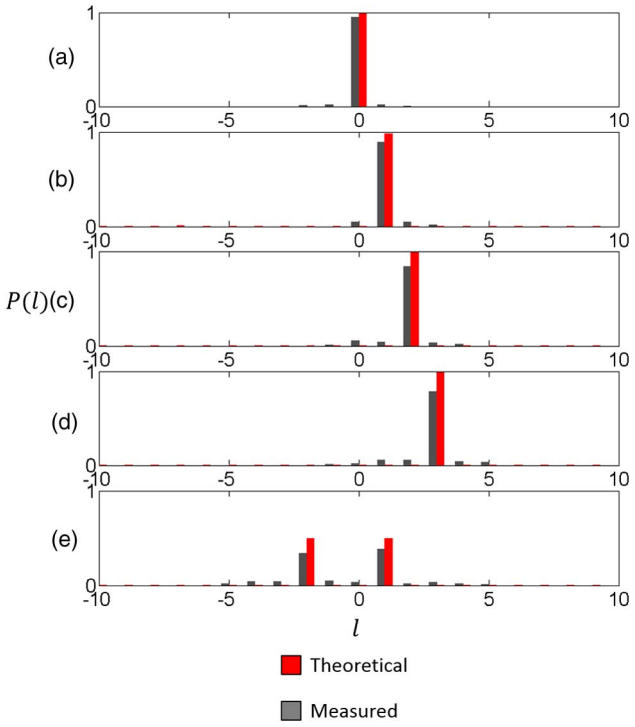

Fig. 4. Mode purity calculated and measured results. (a) $l = 0$; (b) $l = +1$; (c) $l = +2$; (d) $l = +3$; (e) $l = |+1\rangle + |-2\rangle$.

(see Supplement 1), and an increase in the number of steps per phase sector.

One of the potential issues associated with the SPP in the VCSEL aperture is its backreflection. Feedback is known to disturb laser modes. In this case, however, the reflected wave from the SPP top surface also has a spiral phase front that makes the reflected mode orthogonal to the plane wave cavity mode. Hence we expect very little coupling of the reflected light back into the laser mode.

4. CONCLUSION

OAM lasers that emit beams with well-defined individual and superpositions of OAM states have been demonstrated based on single longitudinal and polarization mode VCSEL devices integrated with micro-sized SPPs. Although the generation of OAM beams using SPPs is a well-known technique, our integrated approach enables low-cost wafer-scale fabrication that is especially attractive for array applications [8,9,32,35]. It is conceivable that large-scale fabrication techniques, especially nano-imprinting, could be used to fabricate the integrated SPPs in polymeric materials in a single step, as the total depth of all SPPs is the same regardless of their topological charge.

The ability to emit multiple OAM modes in a concentric fashion is useful for a variety of applications. For example, the production of OAM superposition states is particularly attractive to QKD applications [17,18], by transmitting information encoded in OAM states in one of several mutually unbiased bases [26]. In the future, our method could be extended to emit more OAM states from a single VCSEL device, making this scheme another alternative approach to achieving a free-space quantum communication system [36,37]. We foresee that there may also be applications in other areas, such as optical trapping [38], quantum metrology [39], and remote detection [40,41], where the ability to maintain the coherence between the states is important.

The multi-OAM state emission scheme could be further extended by making electrically isolated concentric VCSEL apertures, each with its own integrated SPP, in order to independently modulate the power of each of the many concentric OAM VCSELs within the device. For example, dual-contact VCSELs that emit two independently switchable beams on the same axis are already commercially available [42]. OAM multiplexed high-capacity optical communications could thus be enabled with the reported modulation bandwidth of VCSELs extending well into several tens of gigahertz [43].

National Basic Research Program of China (2014CB340000); National Natural Science Foundation of China (NSFC) (61490715).

Huanlu Li acknowledges the support of the Chinese Scholarship Council. Xinlun Cai acknowledges the support of the "Young 1000-Talent Plan" by the Government of China.

See Supplement 1 for supporting content.

REFERENCES

1. J. F. Nye and M. V. Berry, "Dislocations in wave trains," Proc. R. Soc. A **336**, 165–190 (1974).
2. L. Allen, M. Beijersbergen, R. Spreeuw, and J. Woerdman, "Orbital angular momentum of light and the transformation of Laguerre-Gaussian laser modes," Phys. Rev. A **45**, 8185–8189 (1992).
3. G. Gibson, J. Courtial, M. Padgett, M. Vasnetsov, V. Pas'ko, S. Barnett, and S. Franke-Arnold, "Free-space information transfer using light beams carrying orbital angular momentum," Opt. Express **12**, 5448–5456 (2004).
4. J. E. Curtis and D. G. Grier, "Structure of optical vortices," Phys. Rev. Lett. **90**, 133901 (2003).
5. S. Fürhapter, A. Jesacher, S. Bernet, and M. Ritsch-Marte, "Spiral interferometry," Opt. Lett. **30**, 1953–1955 (2005).
6. F. Tamburini, B. Thidé, G. Molina-Terriza, and G. Anzolin, "Twisting of light around rotating black holes," Nat. Phys. **7**, 195–197 (2011).
7. A. Mair, A. Vaziri, G. Weihs, and A. Zeilinger, "Entanglement of the orbital angular momentum states of photons," Nature **412**, 313–316 (2001).
8. N. Bozinovic, Y. Yue, Y. Ren, M. Tur, P. Kristensen, H. Huang, A. E. Willner, and S. Ramachandran, "Terabit-scale orbital angular momentum mode division multiplexing in fibers," Science **340**, 1545–1548 (2013).
9. J. Wang, J. Yang, I. M. Fazal, N. Ahmed, Y. Yan, H. Huang, Y. Ren, Y. Yue, S. Dolinar, M. Tur, and A. E. Willner, "Terabit free-space data transmission employing orbital angular momentum multiplexing," Nat. Photonics **6**, 488–496 (2012).
10. Y. F. Yu, Y. H. Fu, X. M. Zhang, A. Q. Liu, T. Bourouina, T. Mei, Z. X. Shen, and D. P. Tsai, "Pure angular momentum generator using a ring resonator," Opt. Express **18**, 21651–21662 (2010).
11. C. R. Doerr and L. L. Buhl, "Circular grating coupler for creating focused azimuthally and radially polarized beams," Opt. Lett. **36**, 1209–1211 (2011).
12. X. Cai, J. Wang, M. J. Strain, B. Johnson-Morris, J. Zhu, M. Sorel, J. L. O'Brien, M. G. Thompson, and S. Yu, "Integrated compact optical vortex beam emitters," Science **338**, 363–366 (2012).
13. K. Iga, "Surface-emitting laser—its birth and generation of new optoelectronics field," IEEE J. Sel. Top. Quantum Electron. **6**, 1201–1215 (2000).
14. L. A. C. Carl Wilmsen and H. Temkin, *Vertical-Cavity Surface-Emitting Lasers: Design, Fabrication, Characterization, and Applications* (Cambridge University, 2001), Vol. **12**, p. 474.
15. B. Zhang, G. S. Solomon, M. Pelton, J. Plant, C. Santori, J. Vučković, and Y. Yamamoto, "Fabrication of InAs quantum dots in AlAs/GaAs DBR pillar microcavities for single photon sources," J. Appl. Phys. **97**, 073507 (2005).
16. J. L. Duligall, M. S. Godfrey, K. A. Harrison, W. J. Munro, and J. G. Rarity, "Low cost and compact quantum key distribution," New J. Phys. **8**, 249 (2006).

17. C. H. Bennett and G. Brassard, "Quantum cryptography: public key distribution and coin tossing," Theor. Comput. Sci. **560**, 7–11 (2014).
18. B. Rodenburg, M. P. J. Lavery, M. Malik, M. N. O'Sullivan, M. Mirhosseini, D. J. Robertson, M. Padgett, and R. W. Boyd, "Influence of atmospheric turbulence on states of light carrying orbital angular momentum," Opt. Lett. **37**, 3735–3737 (2012).
19. J. F. Galisteo-López, M. López-García, A. Blanco, and C. López, "Studying light propagation in self-assembled hybrid photonic-plasmonic crystals by Fourier microscopy," Langmuir **28**, 9174–9179 (2012).
20. M. Harris, C. A. Hill, and J. M. Vaughan, "Optical helices and spiral interference fringes," Opt. Commun. **106**, 161–166 (1994).
21. M. Padgett, "An experiment to observe the intensity and phase structure of Laguerre–Gaussian laser modes," Am. J. Phys. **64**, 77–82 (1996).
22. L. Paterson, M. P. MacDonald, J. Arlt, W. Sibbett, P. E. Bryant, and K. Dholakia, "Controlled rotation of optically trapped microscopic particles," Science **292**, 912–914 (2001).
23. S. N. Khonina, V. V. Kotlyar, V. A. Soifer, K. Jefimovs, and J. Turunen, "Generation and selection of laser beams represented by a superposition of two angular harmonics," J. Mod. Opt. **51**, 761–773 (2004).
24. D. Giovannini, J. Romero, J. Leach, A. Dudley, A. Forbes, and M. Padgett, "Characterization of high-dimensional entangled systems via mutually unbiased measurements," Phys. Rev. Lett. **110**, 143601 (2013).
25. M. J. Padgett, D. Giovannini, M. Lavery, J. Romero, S. M. Barnett, F. Miatto, R. W. Boyd, and J. Leach, "Photon orbital angular momentum: generation, measurement and application to QKD," Proc. SPIE **8542**, 85421P (2012).
26. M. Mafu, A. Dudley, S. Goyal, D. Giovannini, M. McLaren, M. J. Padgett, T. Konrad, F. Petruccione, N. Lütkenhaus, and A. Forbes, "Higher-dimensional orbital-angular-momentum-based quantum key distribution with mutually unbiased bases," Phys. Rev. A **88**, 032305 (2013).
27. R. W. Bowman, G. M. Gibson, A. Linnenberger, D. B. Phillips, J. A. Grieve, D. M. Carberry, S. Serati, M. J. Miles, and M. J. Padgett, "'Red Tweezers': fast, customisable hologram generation for optical tweezers," Comput. Phys. Commun. **185**, 268–273 (2014).
28. M. J. Strain, X. Cai, J. Wang, J. Zhu, D. B. Phillips, L. Chen, M. Lopez-Garcia, J. L. O'Brien, M. G. Thompson, M. Sorel, and S. Yu, "Fast electrical switching of orbital angular momentum modes using ultra-compact integrated vortex emitters," Nat. Commun. **5**, 4856 (2014).
29. M. W. Beijersbergen, R. P. C. Coerwinkel, M. Kristensen, and J. P. Woerdman, "Helical-wavefront laser beams produced with a spiral phaseplate," Opt. Commun. **112**, 321–327 (1994).
30. K. Sueda, G. Miyaji, N. Miyanaga, and M. Nakatsuka, "Laguerre-Gaussian beam generated with a multilevel spiral phase plate for high intensity laser pulses," Opt. Express **12**, 3548–3553 (2004).
31. N. Ahmed, K. M. Birnbaum, B. I. Erkmen, S. Dolinar, M. Tur, and A. E. Willner, "Mode properties and propagation effects of optical orbital angular momentum (OAM) modes in a ring fiber," IEEE Photon. J. **4**, 535–543 (2012).
32. S. Li and J. Wang, "A compact trench-assisted multi-orbital-angular-momentum multi-ring fiber for ultrahigh-density space-division multiplexing (19 rings × 22 modes)," Sci. Rep. **4**, 3853 (2014).
33. M. V. Vasnetsov, V. A. Pas'ko, and M. S. Soskin, "Analysis of orbital angular momentum of a misaligned optical beam," New J. Phys. **7**, 46 (2005).
34. G. A. Turnbull, D. A. Robertson, G. M. Smith, L. Allen, and M. J. Padgett, "The generation of free-space Laguerre-Gaussian modes at millimetre-wave frequencies by use of a spiral phaseplate," Opt. Commun. **127**, 183–188 (1996).
35. Y. Yue, N. Ahmed, H. Huang, Y. Yan, Y. Ren, D. Rogawski, and A. E. Willner, "Reconfigurable orbital-angular-momentum-based switching among multiple 100-Gbit/s data channels," in *Optical Fiber Communication Conference/National Fiber Optic Engineers Conference* (Optical Society of America, 2013), paper OM2G.1.
36. M. Mirhosseini, O. S. Magaña-Loaiza, M. N. O'Sullivan, B. Rodenburg, M. Malik, D. J. Gauthier, and R. W. Boyd, "High-dimensional quantum cryptography with twisted light," arXiv: 1402.7113 (2014).
37. M. Malik and R. W. Boyd, "Quantum imaging technologies," arXiv: 1406.1685 (2014).
38. S. Franke-Arnold, J. Leach, M. J. Padgett, V. E. Lembessis, D. Ellinas, A. J. Wright, J. M. Girkin, P. Ohberg, and A. S. Arnold, "Optical ferris wheel for ultracold atoms," Opt. Express **15**, 8619–8625 (2007).
39. V. D'Ambrosio, N. Spagnolo, L. Del Re, S. Slussarenko, Y. Li, L. C. Kwek, L. Marrucci, S. P. Walborn, L. Aolita, and F. Sciarrino, "Photonic polarization gears for ultra-sensitive angular measurements," Nat. Commun. **4**, 2432 (2013).
40. M. P. J. Lavery, F. C. Speirits, S. M. Barnett, and M. J. Padgett, "Detection of a spinning object using light's orbital angular momentum," Science **341**, 537–540 (2013).
41. D. B. Phillips, M. P. Lee, F. C. Speirits, S. M. Barnett, S. H. Simpson, M. P. J. Lavery, M. J. Padgett, and G. M. Gibson, "Rotational Doppler velocimetry to probe the angular velocity of spinning microparticles," Phys. Rev. A **90**, 011801 (2014).
42. N. Li, C. Xie, W. Luo, C. J. Helms, L. Wang, C. Liu, Q. Sun, S. Huang, C. Lei, K. P. Jackson, and R. F. Carson, "Emcore's 1 Gb/s to 25 Gb/s VCSELs," Proc. SPIE **8276**, 827603 (2012).
43. R. Rodes, M. Mueller, B. Li, J. Estaran, J. B. Jensen, T. Gruendl, M. Ortsiefer, C. Neumeyr, J. Rosskopf, K. J. Larsen, M.-C. Amann, and I. T. Monroy, "High-speed 1550 nm VCSEL data transmission link employing 25 GBd 4-PAM modulation and hard decision forward error correction," J. Lightwave Technol. **31**, 689–695 (2013).